Tuning Inner-Sphere Electron Transfer in a Series of Copper/Nitrosoarene Adducts

Mohammad Amin Askari, Farshid Effaty, Federica Gennarini, Maylis Orio, Nicolas Le Poul, Xavier Ottenwaelder

Inorganic Chemistry

pubs.acs.org/IC Article

Tuning Inner-Sphere Electron Transfer in a Series of Copper/Nitrosoarene Adducts

Mohammad S. Askari, Farshid Effaty, Federica Gennarini, Maylis Orio, Nicolas Le Poul,* and X. Ottenwaelder*

Cite This: https://dx.doi.org/10.1021/acs.inorgchem.9b03175 Read Online

ACCESS | Metrics & More | Article Recommendations | Supporting Information

ABSTRACT: A series of copper/nitrosoarene complexes were created that mimic several steps in biomimetic O_2 activation by copper(I). The reaction of the copper(I) complex of *N,N,N′,N′*-tetramethypropylenediamine with a series of para-substituted nitrosobenzene derivatives leads to adducts in which the nitrosoarene (ArNO) is reduced by zero, one, or two electrons, akin to the isovalent species dioxygen, superoxide, and peroxide, respectively. The geometric and electronic structures of these adducts were characterized by means of X-ray diffraction, vibrational analysis, ultraviolet−visible spectroscopy, NMR, electrochemistry, and density functional theory (DFT) calculations. The bonding mode of the NO moiety depends on the oxidation state of the ArNO moiety: κN for ArNO, mononuclear η^2-NO and dinuclear μ-η^2:η^1 for $ArNO^{\bullet-}$, and dinuclear μ-η^2:η^2 for $ArNO^{2-}$. ^{15}N isotopic labeling confirms the reduction state by measuring the NO stretching frequency (1392 cm^{-1} for κN-ArNO, 1226 cm^{-1} for η^2-$ArNO^{\bullet-}$, 1133 cm^{-1} for dinuclear μ-η^2:η^1-$ArNO^{\bullet-}$, and 875 cm^{-1} for dinuclear μ-η^2:η^2 for $ArNO^{2-}$). The ^{15}N NMR signal disappears for the $ArNO^{\bullet-}$ species, establishing a unique diagnostic for the radical state. Electrochemical studies indicate reduction waves that are consistent with one-electron reduction of the adducts and are compared with studies performed on Cu-O_2 analogues. DFT calculations were undertaken to confirm our experimental findings, notably to establish the nature of the charge-transfer transitions responsible for the intense green color of the complexes. In fine, this family of complexes is unique in that it walks through three redox states of the ArNO moiety while keeping the metal and its supporting ligand the same. This work provides snapshots of the reactivity of the toxic nitrosoarene molecules with the biologically relevant Cu(I) ion.

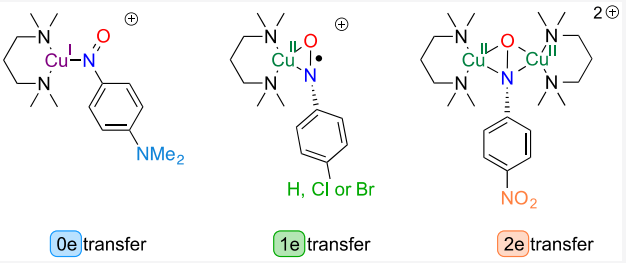

INTRODUCTION

The interaction of nitrosoarenes (ArNO) with metal centers has drawn much attention because of its relevance to biological pathways[1−7] and catalytic C−N bond formation processes.[8−12] Chemists now have a good understanding of the geometric structure of transition metal/nitrosoarene complexes.[13,14] In addition, ArNO species are redox-noninnocent ligands,[15−17] which portends a large landscape of electronic structures and reactivity types upon interaction with redox-active metal ions.

Because ArNO species are isovalent with O_2, the reduction of ArNO by a transition metal is akin to the reduction of O_2 to the superoxide ion ($O_2^{\bullet-}$, 1e reduction) or the peroxide ion (O_2^{2-}, 2e reduction). Therefore, metal/ArNO adducts are often regarded as surrogates for metal/O_2 adducts. In particular, and with relevance to the present paper, the activation of O_2 by Cu(I) centers is paramount in the biological world. This process fuels enzymes such as dopamine-β-hydroxylase, tyrosinase, and particulate methane monooxygenase, to name but a few.[18,19] This has inspired numerous biomimetic studies in which an electron-rich Cu(I) species is reacted with O_2.[20−22] Without protection of the protein backbone, however, the ensuing Cu/O_2 complexes are usually too oxidative to be stable above −60 °C. By contrast, Cu/ArNO adducts have been shown to have geometric and electronic structures very similar to those in Cu/O_2 adducts but were advantageously characterized at ambient temperature.[17,23−25]

Owing to the asymmetric structure of ArNO in comparison with that of O_2, the structural variety of metal/nitrosoarene complexes exceeds that of metal/O_2 compounds. Some of the main bonding modes of ArNO to metal ions are shown in Scheme 1,[13,14] with the most common one being through the N atom (κN). The other bonding modes are thought to be more prevalent when the ArNO moiety is reduced to the mono- or dianion.

The NO bond length in metal/ArNO complexes depends on the bonding mode, nature, and oxidation state of the metal and the supporting ligands but alone is insufficient to characterize

Received: October 29, 2019

Scheme 1. Some Bonding Modes in Metal/Nitrosoarene Complexes, with Typical NO Bond Lengths[13]

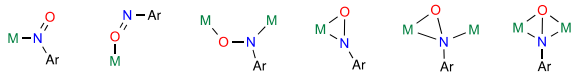

the degree of reduction of the ArNO moiety, as was already shown with metal/O_2 adducts.[26] A few studies have scrutinized the electronic structure on metal/ArNO complexes, particularly the oxidation state of the ArNO moiety, by means of techniques such as X-ray absorption spectroscopy or vibrational analysis with isotopic labeling (Scheme 2 for group 10 and 11 complexes). Their main conclusions are the following:

(i) In the majority of mononuclear κN nitrosoarene complexes, the NO bond length, 1.209−1.31 Å, shows little or no elongation compared with that in free nitrosoarenes,[13,14,27−29] unless back-bonding from the metal becomes significant.[16] A radical character of the κN-ArNO moiety, and thus formally a 1.5 bond order, has been confirmed or inferred in a few species (Scheme 2a).[16,30,31]

(ii) Most mononuclear κO complexes with non-d^{10} transition metals are structurally disordered,[13,14,32−36] and conclusive statements about the extent of back-donation and ArNO reduction cannot be made. By contrast, the non-disordered crystal structures of [(Me_6tren)Cu(κO-PhNO)]X (X = TfO^-, SbF_6^-; Scheme 2b) show significant NO bond elongation. The radical character of the PhNO moiety (to an arylnitrosyl radical anion) was confirmed by magnetic measurements and vibrational and computational studies.[17,37]

(iii) Dinuclear μ-η^1:η^1 (end-on) complexes present varying degrees of ArNO reduction: by 0e (NO = 1.257−1.32 Å),[28,29,38−41] 1e (1.33−1.35 Å),[42] and 2e (1.37−1.49 Å; Scheme 2c).[43,44]

(iv) In η^2-NO complexes, the NO bond length (1.323−1.432 Å)[16,23,31,45−52] is significantly longer than that in free nitrosoarenes. 1e reduction of the ArNO moiety has been confirmed in Cu and Ni complexes (Scheme 2d).[23,52] Further reduction of the Ni complex led to a doubly reduced $PhNO^{2-}$ moiety.[52] 2e reduction of the ArNO moiety was also confirmed in a square-planar Pd(II) species upon reaction of a Pd^0 species with TolNO.[16]

(v) Alongside several $ArNO^{2-}$ examples (N−O = 1.40−1.53 Å),[31,53−58] dinuclear μ-η^2:η^1 complexes have been found in the solid-state structures of Cu complexes with shorter NO bond lengths (1.322−1.375 Å).[23,37] Typically, the 1e-reduced $ArNO^{\bullet-}$ moiety binds η^2 to a Cu(II) center and η^1 to a Cu(I) center (Scheme 2e). These species are thought to be in equilibrium with the mononuclear form [Cu^{II}(η^2-$ArNO^{\bullet-}$)] in solution.[23,37]

(vi) Dinuclear μ-η^2:η^2 complexes are quite rare, and only a few examples with Rh,[57] Zr,[59] Hf,[59] Ni,[23] and Cu[25] are reported in the literature. With an NO bond length in the range of single bonds (1.422−1.500 Å), these complexes possess a doubly reduced $ArNO^{2-}$ moiety. In the case of the Cu complex (Scheme 2f), this 2e reduction was made possible by using a very electron-poor nitrosoarene bearing a *p*-NO_2 substituent. More on this complex will be discussed below.

Scheme 2. Confirmed Examples of Group 10 and 11 Complexes in Which ArNO Gets Reduced by 1e or 2e upon Reaction[a]

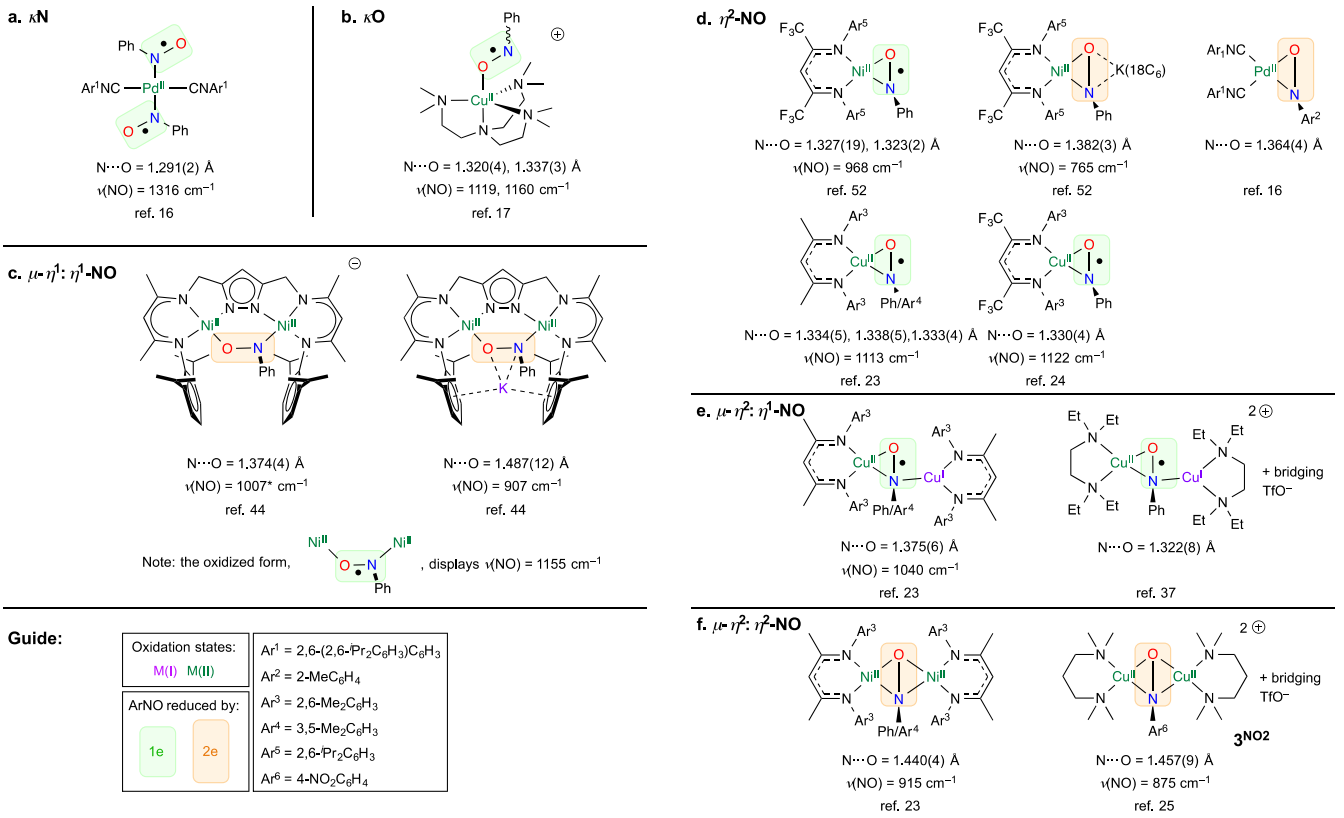

[a]Asterisks indicate calculated values.

https://dx.doi.org/10.1021/acs.inorgchem.9b03175
Inorg. Chem. XXXX, XXX, XXX−XXX

To summarize, 1e reduction of the ArNO moiety is usually indicated by NO bond lengths in the range 1.29−1.37 Å and NO stretching frequencies in the range 1000−1300 cm^{-1} (Scheme 2). Reduction by 2e is revealed by NO bond lengths of 1.36−1.46 Å and NO stretching frequencies below 950 cm^{-1}. When no reduction occurs, the NO bonds are short [1.261(4) and 1.268(4) Å for free PhNO] and the NO stretching frequency is high (1506 cm^{-1} for free PhNO), although these values can be modified significantly when back-bonding is present.[16] Last, 4e reduction of PhNO, with complete NO bond cleavage, is possible with very electron-rich metal complexes such as cobalt(I) β-diketiminate species.[60]

Noting that these examples comprise different supporting ligands and metal ions, we aimed at providing a systematic study of the degree of inner-sphere ArNO reduction by using a single Cu(I) precursor. Thus, in the present study, we report on adducts $\mathbf{3}^{R}$ (R = NMe_2, H, Cl, Br, NO_2) formed upon intermolecular reaction of para-substituted nitrosobenzenes $\mathbf{2}^{R}$ with the Cu(I) complex of *N*,*N*,*N*′,*N*′-tetramethyl-1,3-propanediamine (TMPD), **1** (Scheme 3), for which analogous Cu/O_2 chemistry is known.[61−63]

Scheme 3. Formation of the $\mathbf{3}^{R}$ Adducts[a]

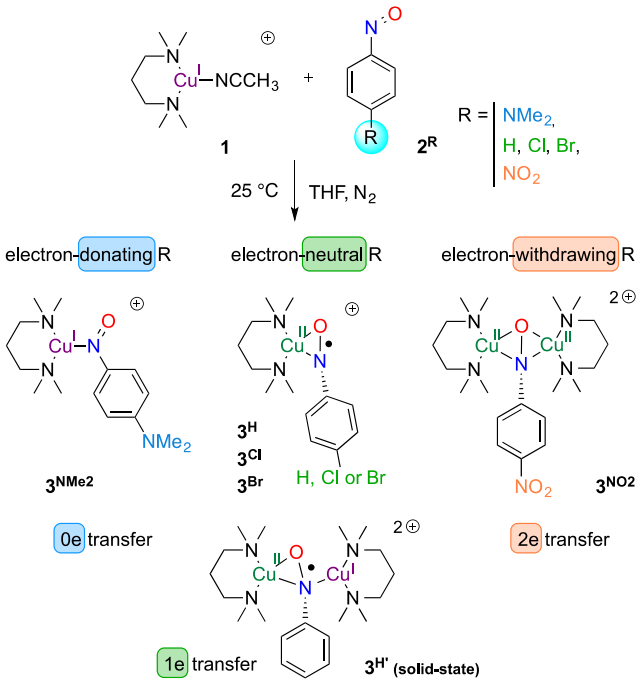

[a]With a TfO^- counterion. $\mathbf{3}^{NO2}$ was already reported.[25]

RESULTS AND DISCUSSION

Synthesis and Crystallography. The slow addition of a $[(MeCN)_4Cu](TfO)$ (MeCN = acetonitrile) solution to a solution of TMPD and nitrosoarene, in a 1:1:1 ratio in tetrahydrofuran (THF) at 25 °C (1:1:2 for R = NO_2), results in the formation of deeply colored complexes that remain stable under inert conditions. Crystallization of the complexes by the slow diffusion of pentane into the reaction mixtures at −30 °C afforded crystals suitable for X-ray diffraction analysis. Several binding motifs consisting of mono- and dinuclear complexes are obtained depending on the para substituent of the nitrosoarene (Figure 1 and Table S1).

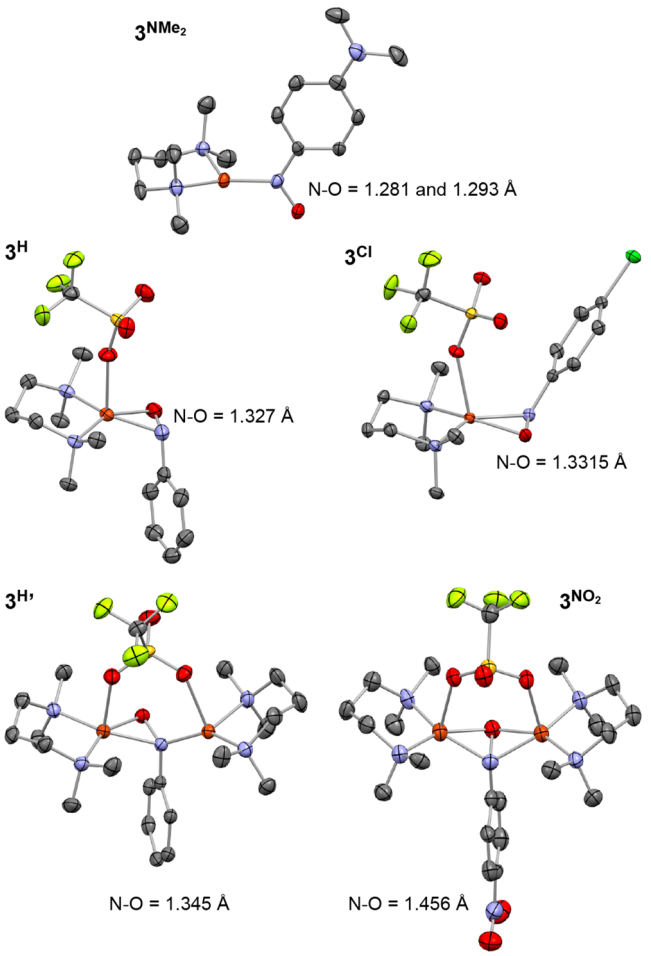

Figure 1. ORTEP at 50% probability of $\mathbf{3}^{NMe_2}$ (one of two independent molecules), $\mathbf{3}^{H}$, $\mathbf{3}^{H'}$, $\mathbf{3}^{Cl}$, and $\mathbf{3}^{NO_2}$, with relevant N−O bond lengths. Uncoordinated TfO^- anions ($\mathbf{3}^{NMe_2}$ and $\mathbf{3}^{NO_2}$) and H atoms were omitted for clarity.

The structure of $\mathbf{3}^{NMe_2}$ is that of a copper(I) arylnitroso complex, i.e., mere κN coordination of $\mathbf{1}^{NMe_2}$ onto the $[TMPDCu^{I}]^+$ complex **1**. The N−O bond lengths in the two independent molecules, 1.281 and 1.293 Å, are typical for N═O double bonds. The trigonal-planar ligand field of Cu is consistent with a Cu(I) oxidation state. In the solid state, the species dimerizes via two weak Cu···O interactions (2.242 and 2.278 Å) between two crystallographically related $\mathbf{3}^{NMe_2}$ cations. This fact, coupled with the back-bonding of Cu into the nitroso π^* orbital, could explain the slight elongation of the N−O bond compared with a true double bond.[16,37]

Two types of crystals were obtained in the same crystallization pot with R = H. The minor component, of green color, is the mononuclear $[TMPDCu^{II}(\eta^2\text{-}PhNO^{\bullet-})(TfO)]$ species ($\mathbf{3}^{H}$). This complex displays an η^2-NO coordination with an elongated N−O bond of 1.327 Å, consistent with a 1.5 bond order.[23,52] Cu sits in a square-pyramidal environment with a TfO^- anion as a weak axial ligand (Cu···O = 2.345 Å). The brown major component, $\mathbf{3}^{H'}$, of the formula $[TMPDCu^{II}(\mu\text{-}\eta^2\text{:}\eta^1\text{-}PhNO^{\bullet-})(\mu\text{-}TfO)\text{-}Cu^{I}TMPD](TfO)$ also displays an elongated N−O bond 1.345 Å, consistent with a 1.5 bond order. One of the Cu centers is bonded to both N and O of the PhNO moiety (Cu−N = 2.019 Å; Cu−O = 1.853 Å), while the other is only bonded to the N atom of PhNO (Cu−N = 1.904 Å; Cu···O =

https://dx.doi.org/10.1021/acs.inorgchem.9b03175
Inorg. Chem. XXXX, XXX, XXX−XXX

2.828 Å). Species $3^{H\prime}$ is therefore well described as formed from the association of the minor green component 3^{H} with one molecule of **1** (Scheme 4). Such architecture and

Scheme 4. Mononuclear/Dinuclear Equilibrium in 3^{H} Species[a]

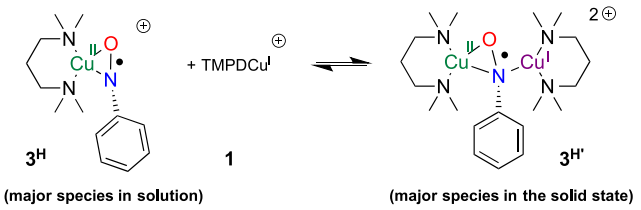

[a]TfO^{-} anions are not shown.

association were already described in the literature.[23,37] Because the mononuclear complex prevails in solution (the solution is green, and a Job titration confirms a 1:1 stoichiometry; Figure S14), formation of the dinuclear compound is an artifact of crystallization.

For 3^{Cl}, only green crystals of $[TMPDCu^{II}(\eta^2\text{-}2^{Cl\bullet-})(TfO)]$ were formed. The molecular structure is very similar to that of 3^{H}, with a 1.5 N−O bond order (1.3315 Å), except that the TfO^{-} anion and the aromatic ring are on the same side of the CuNO plane.

The complex with the most electron-poor ArNO moiety, 3^{NO_2}, was characterized in a previous communication.[25] It is a dinuclear species of the formula $[TMPDCu^{II}(\mu\text{-}\eta^2{:}\eta^2\text{-}PhNO^{2-})(\mu\text{-}TfO)Cu^{II}TMPD](TfO)$, where 2^{NO_2} is reduced by 2e (N−O = 1.456 Å) and both Cu centers are in the 2+ oxidation state.

Overall, the crystallographic study concludes on an increased degree of electron transfer from **1** to 2^{R} inasmuch as the *p*-R substituent is made more electron-poor: 0e in 3^{NMe_2}, 1e in 3^{H}/$3^{H\prime}$ and 3^{Cl}, and 2e in 3^{NO_2}. The lability of Cu complements the self-assembly process by allowing TfO^{-} or extra Cu(I) coordination when necessary.

IR Properties. Vibrational analysis by IR spectroscopy was conducted on 2^{R} precursors and 3^{R} complexes, where the N atom of the nitroso moiety is either ^{14}N or ^{15}N. Synthesis of the ^{15}N-labeled 2^{R} precursors is provided in the Supporting Information. Isotopic labeling enables one to isolate the vibrations near the nitroso moiety from the rest of the molecule. In parallel, density functional theory (DFT) calculations were conducted to identify the nature of the modes observed (especially NO vs CN stretches in the ArNO moiety).

Comparing the IR properties of the organic precursors 2^{R} is tentative because they have different structures in the solid state: monomeric for 2^{NMe_2}, syn dimeric for 2^{H}, and anti dimeric for 2^{Br} (Tables 1 and S2 and Figures S1−S6). Still, the correlation between the experimental and calculated spectra is excellent, providing confidence that the calculations can enable us to locate the NO stretch accurately in the complexes.

Drastic changes in the NO stretching frequency are seen in 3^{R} complexes, consistent with NO bond weakening upon electron transfer (Tables 1 and S3 and Figures S7−S12). While the symmetry of the complexes is different and some complexes have multiple vibrational modes involving the NO stretch, the NO stretching energy decreases from 1315/1392 cm^{-1} for 3^{NMe_2} to 1226 cm^{-1} for 3^{Br} to 875 cm^{-1} for 3^{NO_2}.[25] This trend, supported by DFT calculations, is fully consistent

Table 1. NO Stretching Frequencies[a]

species	ν (Δ)/cm^{-1}	species	ν (Δ)/cm^{-1}
2^{NMe_2}	1365 (12), 1340 (19)	3^{NMe_2}	1392 (14), 1315 (6)
2^{H} [b]	1388 (27)	$3^{H\prime}$ [c]	1162 (10), 1133 (23)
2^{Br} [d]	1286 (4), 1256 (24)	3^{Br}	1226 (6)
2^{NO_2} [d]	1238 (20)	3^{NO_2}	875 (15)

[a]Measured at 25 °C on species labeled with ^{14}N and ^{15}N on the NO moiety. Full data are given in the Supporting Information. [b]Syn ArN(O)N(O)Ar dimer. [c]Contains a small amount of mononuclear species 3^{H}. [d]Anti ArN(O)N(O)Ar dimer.

with reduction of the bond order upon inner-sphere electron transfer from the Cu center(s). For mixed-valent dinuclear species $3^{H\prime}$, the NO stretch is lowered from 3^{Br} by about 70−100 cm^{-1}, consistent with the electron density being delocalized onto the additional Cu(I) center.

NMR Properties. In $CDCl_3$, CD_2Cl_2, or acetone-d_6 solutions, all 3^{R} species display diamagnetic ^{1}H and ^{13}C NMR spectra (Figures S37−S47). For 3^{H}, 3^{Cl}, and 3^{Br}, this indicates a singlet ground state, as was observed for similar η^2-ArNO complexes.[23,24,37] By analogy with structurally similar η^2-superoxocopper(II) species, this ground-state singlet is expected to be highly delocalized.[64] This situation also contrasts with the end-on topology, where end-on superoxocopper(II) complexes have a $S = 1$ ground state,[65−68] as do $Cu^{II}(\kappa O\text{-}ArNO^{\bullet-})$ complexes when Cu−O−N−C_{Ar} is coplanar.[17]

The ^{15}N NMR spectra of the ^{15}N-labeled 3^{R} species are most informative on the degree of electron transfer (Figure 2

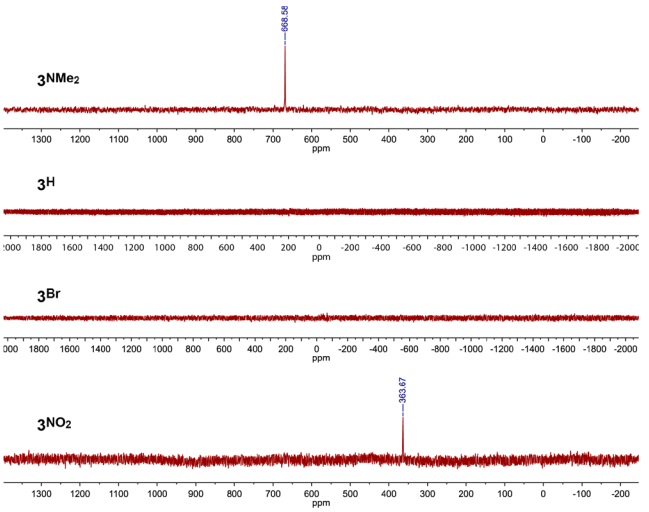

Figure 2. ^{15}N NMR data (50.7 MHz) of the 3^{R} species (R = NMe_2, H, Br, NO_2), ^{15}N-enriched at the NO position, in $CDCl_3$ at 25 °C. Species 3^{H} was made in situ by mixing equimolar amounts of TMPD, $[Cu(MeCN)_4](TfO)$, and 2^{H}.

and Table 2). For comparison, the ^{15}N NMR spectra of the ^{15}N-labeled 2^{R} species reveal a logical downfield shift of the signal inasmuch as the R substituent becomes more electron-poor. Cu(I) coordination on 2^{NMe_2} to form 3^{NMe_2} leads to an upfield shift of the signal by 119 ppm, consistent with the presence of a partial charge transfer from Cu(I) to the ArNO moiety. On the other end of the series, the formation of 3^{NO_2} leads to a dramatic upfield shift of the signal by 550 ppm, consistent with the ArNO moiety being doubly reduced

https://dx.doi.org/10.1021/acs.inorgchem.9b03175
Inorg. Chem. XXXX, XXX, XXX−XXX

Table 2. ^{15}N NMR Data[a]

species	$\delta(^{15}N)$/ppm	species	$\delta(^{15}N)$/ppm
2^{NMe2}	787.58	3^{NMe2}	668.58
2^{H}	885.83	3^{H}	not observed
2^{Br}	878.67	3^{Br}	not observed
2^{NO2}	913.23	3^{NO2}	363.67

[a]Measured in $CDCl_3$ at 25 °C on a 500 MHz instrument; $\nu(^{15}N)$ = 50.7 MHz.

($ArNO^{2-}$) and therefore quite electron-rich. Interestingly, no ^{15}N signal was observed for 3^{H} and 3^{Br} under the same recording conditions or with a wider acquisition window. This behavior is consistent with the radical character of the $ArNO^{\bullet-}$ moiety in these species. A small amount of triplet character admixture in the ground-state singlet at room temperature could lead to a paramagnetic shift of the ^{15}N NMR resonance outside the acquisition window (Fermi contact at ^{15}N).[69] Hence, the lack of a signal in a standard acquisition window can be used as a local diagnostic of radical character on N. Overall, the NMR data confirm, in solution, the assignments that were made in the solid state.

Ultraviolet−Visible (UV−Vis) Absorption Properties. The electronic structure of the complexes was probed by UV−vis absorption spectroscopy (Figure 3 and Table 3).

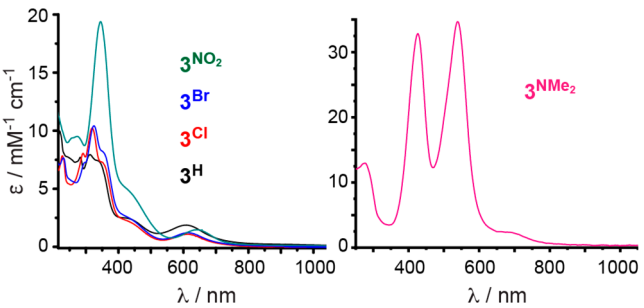

Figure 3. UV−vis spectra of 3^{R} species in CH_2Cl_2 at 25 °C.

Table 3. UV−Vis Data of 3^{R} Complexes[a]

species	λ_{max} (ε)[b]			
3^{NMe_2}	426 (32.8)		538 (34.7)	690 (2.3)
3^{H}	313 (8.0), 338 (7.4)	440 (sh)		609 (1.9)
3^{Cl}	319 (10.2), 350 (7.3)	440 (sh)		614 (1.1)
3^{Br}	325 (10.4), 350 (8.2)	440 (sh)		614 (1.2)
3^{NO_2}	345 (19.4)	440 (sh)		644 (1.5)

[a]Measured in CH_2Cl_2 at 25 °C. [b]λ_{max}/nm (ε/mM^{-1} cm^{-1}).

Complexes 3^{H}, 3^{Cl}, and 3^{Br} display sensibly the same UV−vis spectrum, with an intense band around 330 nm and a less intense feature around 610 nm. Compound 3^{NO^2} exhibits the same spectral shape, but the 345 nm band is twice as intense. The spectrum for complex 3^{NMe^2} is very different from the other four spectra. It shows two very intense bands at 426 and 538 nm, while the weaker feature is red-shifted to 690 nm. These absorptions will be analyzed in the next section.

DFT Calculations. DFT calculations have been undertaken on the 3^{R} complexes to gain insight into the nature of the species observed experimentally and to correlate their electronic structures to the experimental data. The structures of the 3^{R} species were subjected to geometry optimization, and their electronic properties were investigated. A good agreement is found upon a comparison of the molecular geometries with the X-ray crystallographic data (Figure S13). The calculated NO bond lengths are 1.243 Å for 3^{NMe_2}, 1.287−1.288 Å for 3^{H}, 3^{Cl}, and 3^{Br}, 1.313 Å for $3^{H'}$, and 1.405 Å for 3^{NO_2}. While these values are all underestimated (up to 0.05 Å), they lie within the typical error range of DFT and provide a fair trend along the series, being thus informative on the redox state of the ArNO moiety. The DFT-optimized structures are very close to those observed experimentally, with root-mean-square deviations of 0.543, 0.427, 0.407, 0.419, 0.444, and 0.338 from the crystal molecular structures of 3^{NMe_2}, 3^{H}, 3^{Cl}, 3^{Br}, $3^{H'}$, and 3^{NO_2}, respectively.

Time-dependent DFT (TD-DFT) calculations were performed on the 3^{R} complexes, and the predicted spectroscopic data provide calculated spectra that compare well with the experimental observations (Tables S4−S8 and Figures S15−S20). Our computations support that the UV−vis spectra of 3^{H}, 3^{Cl}, 3^{Br}, and 3^{NO_2} are similar and dominated by two main absorption bands of different intensities, while that of 3^{NMe_2} displays two intense electronic transitions. For the latter, the band at 538 nm is assigned to a metal-to-ligand charge transfer (MLCT), and the band at 426 nm is attributed to a ligand-to-ligand charge transfer (LLCT). For both transitions, the acceptor states mainly involve the nitroso moiety (Figure S16). The electronic transitions for 3^{NO_2} were already analyzed.[25] The 345 and 644 nm bands correspond to MLCT transitions involving the μ-η^2:η^2-NO^{2-} moiety, in a very similar manner to the transitions in the (μ-η^2:η^2-O_2^{2-})Cu^{II}_2 cores that mimic the active sites of oxytyrosinase and oxyhemocyanin.[22] For 3^{H}, 3^{Cl}, and 3^{Br}, the absorptions near 320 nm are due to a combination of MLCT and LLCT, with the acceptor state involving the NO moiety, while the transitions in the visible around 610 nm display a mixed character with similar contributions from the metal and the nitroso moiety in both donor and acceptor states (Figures S17−S19). Our TD-DFT calculations thus adequately reproduce the energy of the key features of the experimental spectra, which further support the geometries and electronic properties of the 3^{R} complexes. Vibrational analysis also confirmed the experimental observations (vide supra). Consequently, 3^{NMe_2} can be described as a Cu(I) complex, while 3^{H}, 3^{Cl}, and 3^{Br} are Cu^{II}-($ArNO^{\bullet-}$) species. The dimer $3^{H'}$ is assigned to Cu^{II}−Cu^{I}-($ArNO^{\bullet-}$) species, while 3^{NO_2} was previously shown to be a Cu(II)−Cu(II) complex with a $ArNO^{2-}$ moiety (2e-reduced ArNO).

Electrochemical Studies. Because this work aims at tuning the redox properties by simple substitution, we studied the electrochemical behavior of both precursors 2^{R} and complexes 3^{R} for the whole series of R substituents (NMe_2, H, Cl, Br, and NO_2). The goal was to correlate the electrochemical properties with the reactivity (0e, 1e, or 2e transfer) observed upon reaction with the $[(TMPD)Cu^{I}]^{+}$ complex **1** and the H-atom-transfer (HAT) reactivity of the 3^{R} complexes (see below). The data were also compared to existing records for analogous ArNO and O_2 complexes. Cyclic voltammetry (CV) studies were performed at a glassy-carbon working electrode in dry CH_2Cl_2 with 0.1 M NBu_4OTf as the supporting electrolyte. In what follows, all potentials are referenced to the $Fc^{+/0}$ couple.

Substituted Nitrosoarenes, 2^{R}. CV studies of the free nitrosoarenes, 2^{R}, led to the summary in Scheme 5. 2^{H} was first studied for a comparison with the literature.[70−72] When scanned negatively, it displays two reversible responses at $E^{A}_{1/2}$

https://dx.doi.org/10.1021/acs.inorgchem.9b03175
Inorg. Chem. XXXX, XXX, XXX−XXX

Scheme 5. Reduction Steps of 2^R Species

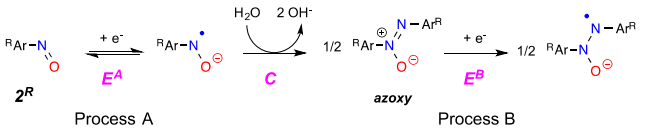

= −1.40 V (process A) and $E^B_{1/2}$ = −1.86 V versus $Fc^{+/0}$ (process B) (Figure S21 and Table 4). An irreversible

Table 4. Electrochemical Data of the 2^R Nitrosoarenes[a]

species	$E^A_{1/2}(2^R)$	$E^B_{1/2}(2^R)$	σ_{para}[b]
2^{NMe_2}	−1.69 (120)[c]	d	−0.83
2^H	−1.40 (90)	−1.86 (100)	0
2^{Cl}	−1.32 (110)	−1.79 (90)	0.227
2^{Br}	−1.30 (90)	−1.75 (90)	0.232
2^{NO_2}	−0.93 (90)	−1.33 (100)[e]	0.78

[a]In CH_2Cl_2 containing 0.1 M NBu_4OTf at 25 °C (glassy-carbon working electrode); scan rate v = 0.1 V s^{-1}, E/V versus $Fc^{+/0}$ (ΔE_p/mV). [b]σ_{para} Hammett parameters. [c]Determined at v = 0.5 V s^{-1}. [d]Not determined. [e]An intermediate wave at −1.17 V was observed at faster scan rates.

oxidation peak is also detected at 0.63 V on the backscan after reduction at −1.90 V (Figure S22). Variation of the scan rate v induces a significant modification of the redox behavior (Figure S23), which is typical of two successive electron-transfer processes coupled to a chemical reaction, namely, an ECE mechanism (E = electrochemical and C = chemical; Scheme 5). In agreement with previous electrochemical studies,[70,71] process A corresponds to the monoelectronic reduction of 2^H (Scheme 5), while process B corresponds to 1e reduction of the azoxybenzene formed in situ by reaction of the radical anion with residual water. This dimerization hypothesis is supported by the ratio of the cathodic peak currents, $i^B_{pc}/i^A_{pc} \approx 0.5$ (assuming similar diffusion coefficients). In addition, the value of $E^B_{1/2}$ is in good agreement with the standard potential values for the azoxy species in organic solvents.[70−72]

The processes described in Scheme 5 occur for 2^R with different para substituents (R = NMe_2, H, Cl, Br, NO_2) but at different redox potentials (Figure S21 and Table 4). Under the same experimental conditions, 2^H, 2^{Cl}, and 2^{Br} display almost the same redox pattern, i.e., one quasi-reversible redox system at ca. $E^A_{1/2}$ = −1.3 V and a second one at ca. $E^B_{1/2}$ = −1.8 V. For 2^{NMe_2}, $E^A_{1/2}$ is shifted negatively by ca. 300 mV with respect to $E^A_{1/2}$ (2^H), and the $(2^{NMe_2})^{\bullet-}$ radical anion is relatively unstable because process A occurs irreversibly for v < 0.2 V s^{-1} (Figure S21a). For 2^{NO_2}, $E^A_{1/2}$ and $E^B_{1/2}$ are shifted positively by ca. 500 mV (Figure S21b).

Thus, a span of +760 mV is observed for $E^A_{1/2}$ upon NMe_2/NO_2 substitution, consistent with the electron-donating/withdrawing properties of the substituents. Fittingly, plots of $E^A_{1/2}$ versus the σ_{para} Hammett parameter follow a linear trend, indicating that the value of the redox potential is mainly controlled by electronic effects (Figure S29).

[Cu(TMPD)(ArNO)](OTf) Complexes 3^R. CV studies of the 3^R complexes (R = NMe_2, H, Br, NO_2) were performed under the same experimental conditions as those for 2^R ligands (Figure 4 and Table 5). Adding 2^R to a solution of **1** under CV monitoring led to the same conclusions as those below (Figure S25). All 3^R complexes display a first irreversible reduction

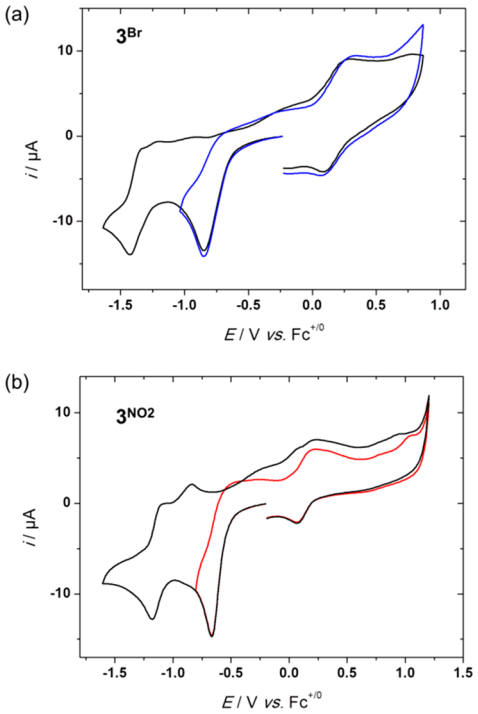

Figure 4. CV cycles at a glassy-carbon working electrode (E/V vs $Fc^{+/0}$; v = 0.1 V s^{-1}) of 3^R (1.0 mM) in dry CH_2Cl_2 and 0.1 M NBu_4OTf: (a) R = Br; (b) R = NO_2.

Table 5. Electrochemical Data of 3^R Complexes[a]

	$E^C_{pc}(3^R)$	$E^D_{1/2}(3^R)$	$E^E_{1/2}(3^R)$	σ_{para}[b]
3^{NMe_2}	−1.05	−1.75	−0.36 (140)	−0.83
3^H	−0.92	−1.45[c]	0.28	0.00
3^{Br}	−0.82	−1.22 (180)	0.08 (130)	0.23
3^{NO_2}	−0.72	−1.17 (145)	0.11 (120)	0.78

[a]In CH_2Cl_2 containing 0.1 M NBu_4OTf at 25 °C; scan rate v = 0.1 V s^{-1}. E/V versus $Fc^{+/0}$ (ΔE_p/mV). [b]σ_{para} Hammett parameters. [c]Irreversible cathodic peak.

peak E^C_{pc} (process C) extending from −1.05 V for 3^{NMe_2} to −0.72 V for 3^{NO_2} (Figure 4 and Table 5). As was the case with process A for the 2^R ligands, the redox potential is mainly controlled by electronic effects, which is confirmed by the linear variation of E^C_{pc} versus σ_{para} Hammett parameters (Figure S29). Whatever the nature of R, the first system remains irreversible at moderate scan rates (v < 10 V s^{-1};Figures 4 and S26 and S27a). This is indicative that a fast chemical reaction occurs upon electrochemical reduction. This EC mechanism was confirmed, for R = NO_2, by the linear behavior of E^C_{pc} versus log v (33 mV $decade^{-1}$; Figure S27b) and the constancy of the normalized current intensity ($i^C_{pc}v^{-1/2}$) with v (inset Figure S27a), hence excluding an ECE process.

CV scanning until −1.8 V leads to the appearance of a second system (process D) at E^D (−1.75 V < E^D < −1.21 V), which is quasi-reversible or irreversible, depending on R (Figures 4 and S31). Increasing the scan rate induces a decrease of the relative peak currents i^C_{pc} and i^D_{pc} (Figure S27c,d for 3^{NO_2}), without modification of the peak potential values. Altogether, this data set confirms that the chemical species that is reduced reversibly through a simple electron transfer at E^D originates from the first electrochemical reduction of the 3^R complex. As shown in Table 5, the potential value at E^D is

https://dx.doi.org/10.1021/acs.inorgchem.9b03175
Inorg. Chem. XXXX, XXX, XXX−XXX

highly dependent on the substituting group R, meaning that the chemical species or complex contains the ArNO moiety. Possibly, reduction of the complex induces breaking of the Cu−ArNO bond, liberating $\mathbf{2^R}$ and explaining the similarity of the E^D and E^A values. Such a hypothesis is verified in all cases except for $\mathbf{3^{NO_2}}$ (Figures S28 and S30).

Exhaustive electrolyses at E^C_{pc} and coulometric measurements confirm that system C is a 1e process per mole of $\mathbf{3^R}$. For example, electrochemical reduction of $\mathbf{3^{NMe_2}}$ leads to its disappearance, while a new wave appears at $E^D_{1/2}$ (Figure S31), together with a significant color change of the solution (purple to orange). A new system also appears in oxidation at −0.2 , +0.45, and +0.65 V, suggesting a release of TMPD (Figure S25a).

In a general manner, 1e reduction of the $\mathbf{3^R}$ complexes is accompanied by fast chemical processes that lead to partial decomplexation and release of the TMPD ligand and/or $\mathbf{2^R}$. The transient electron-reduced species may thus be implicated in several reactions: radical dimerization and simple decoordination, which themselves seem dependent on R.

On the oxidation side, a quasi-reversible system (process E) is detected at $E^E_{1/2}$ (Table 5), with varying peak potential and intensity values as R is varied. $E^E_{1/2}$ is in the same range as that reported by Warren et al. (E_{pa} = +0.48 V in MeCN) for a similar side-on arylnitrosylcopper(II) complex with a diketiminate ligand.[23]

The reduction data obtained for the $\mathbf{3^R}$ complexes can be compared with the few redox processes reported for Ni_n/ArNO and Cu_n/O_2 analogues (Table 6). The side-on arylnitrosyl $\mathbf{3^H}$ species (entry 1) gets reduced at a potential similar to that of Warren's side-on arylnitrosylnickel(II) complex.[52] When ArNO binds in a 1,2-fashion (end-on) between two Ni(II) centers, the potential for $ArNO^{2-/\bullet-}$ conversion is decreased by ca. 650 mV (entry 3).[44] Comparing ArNO with O_2 complexes would be interesting, but so far there is no reported redox data for monocopper superoxo species that would be similar in structure to $\mathbf{3^H}$. The exception is the recent work by Reinaud et al., which showed by spectroelectrochemistry that an in situ generated calix[6]amino-tren end-on superoxo complex could not be reduced above −0.90 V versus Fc at −60 °C (113 K) in acetone.[73] On the other hand, a few dicopper peroxo and superoxo species have been well characterized by electrochemistry with the help of low-temperature approaches (entries 4−7). Here, the irreversible 1e reduction of $\mathbf{3^R}$ is comparable to the monoelectronic and reversible electron-exchange reactions detected for the end-on superoxo/peroxo pyrazolate- and xylO-based complexes (entries 4 and 5).[74,75] Interestingly, the reduction potential of $\mathbf{3^{NO_2}}$ (entry 8) is close to that of Kodera's side-on peroxodicopper(II) species (entry 7), although the latter is a 2e process.[76] Overall, using such comparisons to make educated assignments of the electrochemical processes remains tentative given the large variety of ligands, charge, nuclearity, and bonding topology of the reported complexes. While data for μ-hydroxodicopper complexes that are reminiscent of Cu_n/O_2 species is readily available,[77−82] comparisons with the $\mathbf{3^R}$ complexes would be even more tentative.

HAT Reactivity. We evaluated the reactivity of $\mathbf{3^{Cl}}$, $\mathbf{3^{Br}}$, and $\mathbf{3^{NO_2}}$ for HAT reactivity (Scheme 6). In previous work, Warren et al. reported a Ni^{II}-(η^2-$ArNO^{\bullet-}$) that converts into the related Ni^{II}-(η^2-ArN(H)O) complex (protonated hydroxylamine) upon reaction with 9,10-dihydroanthracene (DHA).[52] Conversely, Meyer et al. reported a dinuclear Ni^{II}_2-(μ-η^1:η^1-ArN(H)O) species that released its H atom to a phenoxyl radical to form the related Ni^{II}_2-(μ-η^1:η^1-$ArNO^{\bullet-}$) species and evaluated a bond dissociation energy BDE(N−H) of around

Table 6. Electrochemical Data of $\mathbf{3^R}$ and Related Ni_n/ArNO and Cu_n/O_2 Complexes

Entry	Reaction [a]	E [b]	Ref.
1	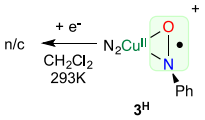	-0.92 [c]	This work
2	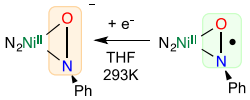	-0.89 [d]	52
3	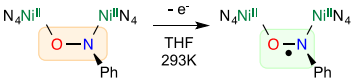	-1.53 [e]	44
4	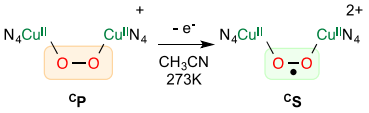	-0.59 [e]	74
5	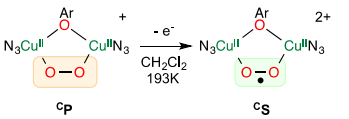	-0.36 [e]	75
6	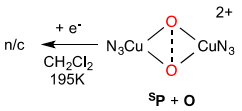	-0.01 [d,f]	82
7	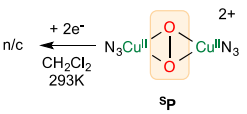	-0.75 [c]	76
8	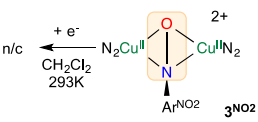	-0.72 [c]	This work

[a]The reaction is written in a way it was carried out either as an oxidation or as a reduction. Abbreviations: n/c, compound not characterized; ^{C}**P**, cis-end-on peroxo; ^{C}**S**, cis-end-on peroxo; ^{S}**P**, side-on peroxo; **O**, bis(μ-oxo). [b]Potential versus $Fc^{+/0}$. [c]Irreversible cathodic peak. [d]Reversible reduction. [e]Reversible oxidation. [f]Converted from the value versus saturated calomel electrode (SCE) using $E_{1/2}(Fc^{+/0})$ = 560 mV versus SCE in these conditions.

Scheme 6. Thermodynamic Analysis of HAT Reactivity

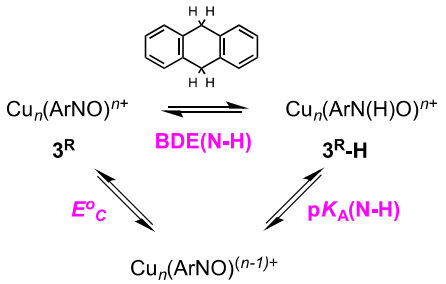

$$BDFE(DHA\text{-}H) = 1.47pK_A + 23.06E^o_C + C \quad \text{(Eqn. 1)}$$

https://dx.doi.org/10.1021/acs.inorgchem.9b03175
Inorg. Chem. XXXX, XXX, XXX−XXX

62−65 kcal mol^{-1}).[44] Following these examples, we reacted to $\mathbf{3}^{Cl}$, $\mathbf{3}^{Br}$, and $\mathbf{3}^{NO_2}$ with DHA (bond dissociation free energy BDFE = 76.0 mol^{-1})[83] under UV−vis monitoring. A significant decrease of the $\mathbf{3}^{R}$ spectrum was observed upon the addition of 40 mol equiv of DHA in THF at 45 °C, which was corrected for self-decomposition of the $\mathbf{3}^{R}$ complexes at this temperature. By analogy with the above examples, we presume that the reaction yielded complexes of ArN(H)O, labeled $\mathbf{3}^{R}$-**H** hereafter (Scheme 6), but their instability prevented further analysis of the reaction and its mechanism.

The electron-withdrawing NO_2 group induces a faster oxidation of DHA, consistent with $\mathbf{3}^{NO_2}$ being a stronger oxidant (higher $E^{C}_{1/2}$) than $\mathbf{3}^{Br}$ and $\mathbf{3}^{Cl}$. The initial rates of reaction depend on the R substituent: 0.029, 0.021, and 0.051 ± 0.005 mM min^{-1} for $\mathbf{3}^{Cl}$, $\mathbf{3}^{Br}$, and $\mathbf{3}^{NO_2}$, respectively. Using eq 1 (Scheme 6)[83] with a temperature correction, the value of $E^{C}_{1/2}$ for $\mathbf{3}^{R}$ taken as E^{C}_{pc}, and using C = 66 kcal mol^{-1} in THF,[84] the pK_A value of the N−H bond in $\mathbf{3}^{R}$-**H** is evaluated around 18 and 19.5 for the NO_2 and Br adducts, respectively, in order to perform HAT from DHA. Similarly, $\mathbf{2}^{NO_2}$ reacts, but slowly, with 1,2-diphenylhydrazine (BDFE = 67.1 kcal mol^{-1}) at 25 °C. This brings the pK_A value to around 13, but this reaction is complicated by the byproduct azobenzene, which can interact with Cu(I) and dissociate $\mathbf{2}^{NO_2}$. Further studies with different substrates are necessary to decipher how nitrosarene complexes perform this reaction, i.e., in a concerted or sequential manner.[85,86]

■ CONCLUSIONS

In summary, placing a synthetic handle at the para position of nitrosoarenes enables control over the degree of electron transfer from Cu(I) complexes, from 0e with electron-donating substituents to 1e with electron-neutral substituents and 2e with electron-poor substituents. As the Cu/ArNO adducts are undergoing self-assembly, the geometric preferences of the Cu center will prevail.[37] Thus, Cu(I) will be found in trigonal geometries, with κN-ArNO coordination, whereas a square-pyramidal Cu(II) will force η^2-ArNO$^{\bullet-/2-}$ coordination. One of the novel features of this work is the use of ^{15}N NMR as a direct, local probe for the redox level of the ArNO moiety. Thus, the absence of a ^{15}N NMR signal coincides with the radical state. A side effect of the self-assembly is, however, the relative instability of the adducts upon external electron-transfer events. Notwithstanding, this series of complexes provides structural snapshots of the isovalent Cu/O_2 chemistry, without the complication of thermal sensitivity of Cu/O_2 species. It also enables redox studies to be performed, although much remains to be done before a proper ArNO/O_2 redox benchmark can be established. This series also highlights the variety of intermediates that could occur during Cu-catalyzed ArNO transformations and suggests that, perhaps, bond-forming events from ArNO precursors may proceed via radical states.

■ EXPERIMENTAL SECTION

Materials. Chemicals were obtained from Sigma-Aldrich and Alfa Aesar, except acetanilide-^{15}N, which was purchased from Cambridge Isotope Laboratories. Air-sensitive samples were handled under an inert atmosphere (N_2) in a dry nitrogen glovebox (O_2 < 0.1 ppm; H_2O < 0.1 ppm) or using standard Schlenk techniques. Solvents were dried by standard procedures, degassed, and stored over 4 Å molecular sieves in the glovebox. *N,N,N′,N′*-Tetramethyl-1,3-propanediamine (TMPD) was distilled over CaH_2 under nitrogen and stored in the glovebox. The copper salt [(MeCN)$_4$Cu](TfO) was prepared by adapting the Kubas procedure using TfOH.[87] 4-Dimethylaminonitrosobenzene ($\mathbf{2}^{NMe_2}$),[88,89] 4-chloronitrosobenzene ($\mathbf{2}^{Cl}$),[90] 4-bromosonitrobenzene ($\mathbf{2}^{Br}$),[90] and 4-nitrosonitrobenzene ($\mathbf{2}^{NO_2}$)[91] were prepared via literature procedures. Isotopically labeled ^{15}N-4-nitrosonitrobenzene and [(TMPDCu)$_2$(μ-TfO)(μ-η^2:η^2-*p*-NO_2-C_6H_4NO)](TfO) were prepared following the procedure reported earlier.[25] 4-Bromoaniline-^{15}N was prepared from ^{15}N-acetamide as reported in the Supporting Information. ^{15}N derivatives of $\mathbf{2}^{H}$, $\mathbf{2}^{Cl}$, and $\mathbf{2}^{Br}$ were prepared similarly to the ^{14}N samples (see the Supporting Information).[90]

Characterization Methods. NMR spectra were recorded on a Varian Innova-500 MHz instrument. All spectra were recorded in $CDCl_3$ unless otherwise noted. ^{1}H and ^{13}C NMR spectra were referenced to internal tetramethylsilane. For $\mathbf{3}^{R}$ species, the signal for the TfO$^-$ anion is not reported; it is observed at 119.5 ppm in concentrated samples. ^{15}N NMR spectra were referenced to external formamide in dimethyl sulfoxide. IR spectra were recorded on a Nicolet iS5 (Thermo Scientific) attenuated-total-reflectance instrument. UV−vis spectra were recorded on an Agilent 8453 spectrophotometer or a B&W Tek i-Trometer. Elemental analysis was performed by the Laboratoire d'Analyze Élémentaire de l'Université de Montréal. The presence of F atoms in the samples interfered with the normal integration peak for H atoms. The value for H is not necessarily trustworthy.

X-ray Crystallography. Crystallographic analysis was performed on a Bruker APEX-DUO diffractometer. The frames were integrated with the Bruker *SAINT* software package using a narrow-frame algorithm. Data were corrected for absorption effects using the multiscan method (*SADABS* or *TWINABS*). The structures were solved by direct methods and refined using the *APEX3* software package. All non-H atoms were refined with anisotropic thermal parameters. H atoms were generated in idealized positions, riding on the carrier atoms with isotropic thermal parameters.

Electrochemistry. Room temperature electrochemical studies of the nitrosoarene ligands and their copper complexes were performed in a glovebox (Jacomex; O_2 < 1 ppm and H_2O < 1 ppm) with a home-designed three-electrode cell (WE, glassy carbon or platinum; RE, platinum wire in a Fc$^+$/Fc solution; CE, platinum or graphite rod). Ferrocene was added at the end of the experiments to determine the redox potential values. The potential of the cell was controlled by an AUTOLAB PGSTAT 100 (Metrohm) potentiostat monitored by the *NOVA 1.11* software. Dichloromethane (Acros) was distilled over CaH_2 under an inert atmosphere and stored in a glovebox. The supporting salt NBu_4PF_6 was synthesized from NBu_4OH (Acros) and HPF_6 (Aldrich). It was then purified, dried under vacuum for 48 h at 100 °C, and then kept under argon in the glovebox. NBu_4OTf (Aldrich, 99%) was stored as received in the glovebox. Electrolytic solutions were prepared in the glovebox and dried for a few days under molecular sieves (3 Å) to remove traces of water before use.

Computational Details. All theoretical calculations were performed with the *ORCA* program package.[92] Full geometry optimizations were carried out for all complexes using the generalized gradient approximation functional BP86[93−95] in combination with the TZV/P[96] basis set for all atoms and by taking advantage of the resolution of the identity (RI) approximation in the Split-RI-J variant[97] with the appropriate Coulomb fitting sets.[98] Increased integration grids (Grid4 in the *ORCA* convention) and tight self-consistent-field convergence criteria were used. IR spectra were obtained from numerical frequency calculations performed on DFT-optimized structures. Isotope shift effects (^{14}N/^{15}N) were taken into account using the *orca_vib* utility program, and vibrational normal modes were visualized with *Chemcraft*[99] software. Solvent effects were accounted for according to the experimental conditions. For that purpose, we used the CH_2Cl_2 (ϵ = 9.08) solvent within the framework of the conductor-like screening (COSMO) dielectric continuum approach.[100] Single-point optical properties were predicted from additional single-point calculations using the same functional/basis set as that employed previously. Electronic transition energies and dipole moments for all models were calculated using TD-DFT[101−103] within

https://dx.doi.org/10.1021/acs.inorgchem.9b03175
Inorg. Chem. XXXX, XXX, XXX−XXX

the Tamm−Dancoff approximation.[104,105] To increase the computational efficiency, the RI approximation[106] was used to calculate the Coulomb term. At least 40 excited states were calculated in each case, and difference transition density plots were generated for each transition. For each transition, difference density plots were generated using the *ORCA* plot utility program and visualized with the *Chemcraft* program. The same procedure was also employed to generate and visualize spin-density plots as well as molecular orbitals.

Synthetic Procedures. *General Procedure for the Synthesis of 3^R Complexes (R = NMe_2, H, Cl, Br).*[25] To a stirring solution of TMPD (0.28 mmol, 1.1 equiv) and the corresponding nitrosobenzene 2^R (0.27 mmol, 1.05 equiv) in 5 mL of THF was added dropwise at 25 °C a solution of $[(MeCN)_4Cu](TfO)$ (0.26 mmol, 1 equiv) in 2 mL of THF. The solution was stirred for 15 min and then cooled to −30 °C. Dropwise addition of the solution to 15 mL of swirling pentane previously cooled to −30 °C resulted in the precipitation of a solid. The solid was isolated, washed with diethyl ether and pentane, and dried in vacuo (yields typically 70−85%). Crystals suitable for X-ray structure determination were grown through the slow layered diffusion of pentane into a concentrated solution of the complex in THF at −30 °C.

[(TMPDCu)(TfO)(κN-p-NMe_2-C_6H_4NO)](TfO) (3^{NMe_2}). Yield: dark purple solid. ^{1}H NMR (500 MHz, $CDCl_3$): δ_{ppm} 1.76 (m, 2H), 2.51 (s, 12H), 2.84 (m, 4H), 3.22 (s, 6H), 6.81 (br, 2H), 9.09 (very br, 2H). ^{13}C NMR (125 MHz, $CDCl_3$): δ_{ppm} 22.89, 40.80, 48.69, 61.75, 112.2, 122.05, 156.26, 158.23. ^{15}N NMR (50.7 MHz, $CDCl_3$): δ_{ppm} 668.58 (NO moiety). Anal. Calcd for $C_{16}H_{28}CuF_3N_4O_4S$: C, 38.98; H, 5.72; N, 11.36; S, 6.50. Found: C, 37.86; H, 5.82; N, 11.13; S, 6.61.

[(TMPDCu)$_2$(μ-TfO)(μ-η^2:η^1-PhNO)](TfO) ($3^{H\prime}$). Yield: brown solid. ^{1}H NMR (500 MHz, $CDCl_3$): δ_{ppm} 1.72 (br, 4H), 2.55 (br, 24H), 2.69 (br, 8H), 7.49 (t, 2H), 7.67 (t, 1H), 8.09 (d, 2H). ^{13}C NMR (125 MHz, $CDCl_3$): δ_{ppm} 22.36, 48.59, 60.59, 120.97 (d upon ^{15}N labeling, $J(^{13}C-^{15}N)$ = 3 Hz), 130.94 (d upon ^{15}N labeling, $J(^{13}C-^{15}N)$ = 2 Hz), 131.78, 160.93. Anal. Calcd for $C_{22}H_{41}Cu_2F_6N_5O_7S_2$: C, 33.33; H, 5.21; N, 8.83; S, 8.09. Found: C, 31.28; H, 5.35; N, 8.37; S, 8.19 (precision is lacking because this compound contains a minor quantity of 3^H in the solid state).

[(TMPDCu)(TfO)(η^2-PhNO)](TfO) (3^H). Yield: prepared in situ (green solution). ^{1}H NMR (500 MHz, $CDCl_3$): δ_{ppm} 1.69 (br, 2H), 2.47 (12H), 2.63 (4H), 7.43 (t, 2H), 7.63 (t, 1H), 7.97 (d, 2H). ^{13}C NMR (125 MHz, $CDCl_3$): δ_{ppm} 20.37, 46.59, 59.24, 119.34 (d upon ^{15}N labeling, $J(^{13}C-^{15}N)$ = 5 Hz), 127.97 (d upon ^{15}N labeling, $J(^{13}C-^{15}N)$ = 2 Hz), 130.78, 160.67 (d upon ^{15}N labeling, $J(^{13}C-^{15}N)$ = 6 Hz). ^{15}N NMR (50.7 MHz, $CDCl_3$): not observed.

[(TMPDCu)(TfO)(η^2-p-ClC_6H_4NO)](TfO) (3^{Cl}). Yield: green solid. ^{1}H NMR (500 MHz, acetone-d_6): δ_{ppm} 2.42 (br, 2H), 3.06 (s, 12H), 3.45 (br, 4H), 7.77 (d, 2H), 7.97 (d, 2H). ^{13}C NMR (125 MHz, acetone-d_6): δ_{ppm} 20.17, 43.19, 55.50, 122.16, 126.10, 130.01, 166.47. Anal. Calcd for $C_{14}H_{22}ClCuF_3N_3O_4S$: C, 34.71; H, 4.58; N, 8.67; S, 6.62. Found: C, 34.27; H, 4.49; N, 8.16; S, 6.38.

[(TMPDCu)(TfO)(η^2-p-Br-C_6H_4NO)](TfO) (3^{Br}). Yield: green solid. ^{1}H NMR (500 MHz, $CDCl_3$): δ_{ppm} 1.74 (br, 2H), 2.65 (br, 12H), 2.78 (br, 4H), 7.54 (d, 2H), 7.91 (d, 1H). ^{13}C NMR (125 MHz, $CDCl_3$): δ_{ppm} 22.28, 48.52, 60.29, 122.81 (d upon ^{15}N labeling, $J(^{13}C-^{15}N)$ = 5 Hz), 126.01, 133.55 (d upon ^{15}N labeling, $J(^{13}C-^{15}N)$ = 2.5 Hz), 160.59 (d upon ^{15}N labeling, $J(^{13}C-^{15}N)$ = 5 Hz). ^{15}N NMR (50.7 MHz, $CDCl_3$): not observed. Anal. Calcd for $C_{14}H_{22}BrCuF_3N_3O_4S$: C, 31.80; H, 4.19; N, 7.95; S, 6.06. Found: C, 31.29; H, 4.49; N, 7.81; S, 6.37.

X-ray data for 3^{NMe_2}, 3^H, $3^{H\prime}$, and 3^{Cl} are available as CCDC 1959040−1959043, respectively. Note that 3^{NO_2} is CCDC 1029423.

■ ASSOCIATED CONTENT

Supporting Information

The Supporting Information is available free of charge at https://pubs.acs.org/doi/10.1021/acs.inorgchem.9b03175.

Experimental supplements, including a crystallography table, a Job plot, ^{15}N labeling, IR data, electrochemistry supplements, DFT data, and NMR spectra (PDF)

Accession Codes

CCDC 1959040−1959043 contain the supplementary crystallographic data for this paper. These data can be obtained free of charge via www.ccdc.cam.ac.uk/data_request/cif, or by emailing data_request@ccdc.cam.ac.uk, or by contacting The Cambridge Crystallographic Data Centre, 12 Union Road, Cambridge CB2 1EZ, UK; fax: +44 1223 336033.

■ AUTHOR INFORMATION

Corresponding Authors

Nicolas Le Poul − *Laboratoire de Chimie, Électrochimie Moléculaires et Chimie Analytique, UMR, CNRS 6521, Université de Bretagne Occidentale, Brest 29238, France;* orcid.org/0000-0002-5915-3760; Email: nicolas.lepoul@univ-brest.fr

X. Ottenwaelder − *Department of Chemistry and Biochemistry, Concordia University, Montreal, Quebec H3G 1M8, Canada;* orcid.org/0000-0003-4775-0303; Email: dr.x@concordia.ca

Authors

Mohammad S. Askari − *Department of Chemistry and Biochemistry, Concordia University, Montreal, Quebec H3G 1M8, Canada;* orcid.org/0000-0002-1746-5141

Farshid Effaty − *Department of Chemistry and Biochemistry, Concordia University, Montreal, Quebec H3G 1M8, Canada;* orcid.org/0000-0002-2389-4903

Federica Gennarini − *Department of Chemistry and Biochemistry, Concordia University, Montreal, Quebec H3G 1M8, Canada; Laboratoire de Chimie, Électrochimie Moléculaires et Chimie Analytique, UMR, CNRS 6521, Université de Bretagne Occidentale, Brest 29238, France;* orcid.org/0000-0001-5679-512X

Maylis Orio − *Aix Marseille Université, CNRS, Centrale Marseille, iSm2, Marseille 13007, France;* orcid.org/0000-0002-9317-8005

Complete contact information is available at: https://pubs.acs.org/10.1021/acs.inorgchem.9b03175

Author Contributions

The manuscript was written through contributions of all authors. All authors have given approval to the final version of the manuscript.

Funding

Financial support was provided by the Natural Sciences and Engineering Council of Canada (Discovery Grant for X.O. and graduate scholarship to M.S.A.) and the Centre de Chimie Verte et Catalyze (Quebec). The authors are also thankful for French financial support through Grant ANR-13-BSO7-0018 and thank the University of Bretagne Occidentale for a mobility grant (F.G.).

Notes

The authors declare no competing financial interest.

■ ACKNOWLEDGMENTS

We thank the Capobianco lab and Biofins platform (Concordia) for help with IR spectral measurement and analysis and Alexey Denisov (Concordia) for help with ^{15}N NMR.

https://dx.doi.org/10.1021/acs.inorgchem.9b03175
Inorg. Chem. XXXX, XXX, XXX−XXX

REFERENCES

(1) Kiese, M. The biochemical production of ferrihemoglobin-forming derivatives from aromatic amines, and mechanisms of ferrihemoglobin formation. *Pharmacol. Rev.* **1966**, *18* (3), 1091.

(2) Eyer, P. Detoxication of N-Oxygenated Arylamines in Erythrocytes. an Overview. *Xenobiotica* **1988**, *18* (11), 1327−1333.

(3) O'Brien, P. J.; Wong, W. C.; Silva, J.; Khan, S. Toxicity of nitrobenzene compounds towards isolated hepatocytes: dependence on reduction potential. *Xenobiotica* **1990**, *20* (9), 945−955.

(4) Kumar, M. R.; Zapata, A.; Ramirez, A. J.; Bowen, S. K.; Francisco, W. A.; Farmer, P. J. Nitrosyl hydride (HNO) replaces dioxygen in nitroxygenase activity of manganese quercetin dioxygenase. *Proc. Natl. Acad. Sci. U. S. A.* **2011**, *108* (47), 18926−18931.

(5) Doctorovich, F.; Bikiel, D. E.; Pellegrino, J.; Suárez, S. A.; Martí, M. A. Reactions of HNO with Metal Porphyrins: Underscoring the Biological Relevance of HNO. *Acc. Chem. Res.* **2014**, *47* (10), 2907−2916.

(6) Doctorovich, F.; Bikiel, D. E.; Pellegrino, J.; Suárez, S. A.; Martí, M. A. How to Find an HNO Needle in a (Bio)-Chemical Haystack. *Progress in Inorganic Chemistry*; John Wiley & Sons, Inc., 2014; Vol. *58*, pp 145−184.

(7) Miao, Z.; King, S. B. Recent advances in the chemical biology of nitroxyl (HNO) detection and generation. *Nitric Oxide* **2016**, *57*, 1−14.

(8) Otsuka, S.; Aotani, Y.; Tatsuno, Y.; Yoshida, T. Aromatic nitroso compounds as.pi. acids in the zerovalent nickel triad metal complexes and the metal-assisted atom-transfer reactions with donor reagents. *Inorg. Chem.* **1976**, *15* (3), 656−660.

(9) Srivastava, R. S.; Khan, M. A.; Nicholas, K. M. Nitrosoarene−Cu(I) Complexes Are Intermediates in Copper-Catalyzed Allylic Amination. *J. Am. Chem. Soc.* **2005**, *127* (20), 7278−7279.

(10) Srivastava, R. S.; Tarver, N. R.; Nicholas, K. M. Mechanistic Studies of Copper(I)-Catalyzed Allylic Amination. *J. Am. Chem. Soc.* **2007**, *129* (49), 15250−15258.

(11) Ho, C.-M.; Lau, T.-C. Copper-catalyzed amination of alkenes and ketones by phenylhydroxylamine. *New J. Chem.* **2000**, *24* (11), 859−863.

(12) Adam, W.; Krebs, O. The Nitroso Ene Reaction: A Regioselective and Stereoselective Allylic Nitrogen Functionalization of Mechanistic Delight and Synthetic Potential. *Chem. Rev.* **2003**, *103* (10), 4131−4146.

(13) Lee, J.; Chen, L.; West, A. H.; Richter-Addo, G. B. Interactions of Organic Nitroso Compounds with Metals. *Chem. Rev.* **2002**, *102* (4), 1019−1066.

(14) Xu, N.; Richter-Addo, G. B. Interactions of Nitrosoalkanes/arenes, Nitrosamines, Nitrosothiols, and Alkyl Nitrites with Metals. *Progress in Inorganic Chemistry*; John Wiley & Sons, Inc., 2014; Vol. *59*, pp 381−446.

(15) Zuman, P.; Shah, B. Addition, Reduction, and Oxidation Reactions of Nitrosobenzene. *Chem. Rev.* **1994**, *94* (6), 1621−1641.

(16) Tomson, N. C.; Labios, L. A.; Weyhermüller, T.; Figueroa, J. S.; Wieghardt, K. Redox Noninnocence of Nitrosoarene Ligands in Transition Metal Complexes. *Inorg. Chem.* **2011**, *50*, 5763−5776.

(17) Askari, M. S.; Girard, B.; Murugesu, M.; Ottenwaelder, X. The two spin states of an end-on copper(II)-superoxide mimic. *Chem. Commun.* **2011**, *47* (28), 8055−8057.

(18) Solomon, E. I.; Heppner, D. E.; Johnston, E. M.; Ginsbach, J. W.; Cirera, J.; Qayyum, M.; Kieber-Emmons, M. T.; Kjaergaard, C. H.; Hadt, R. G.; Tian, L. Copper Active Sites in Biology. *Chem. Rev.* **2014**, *114* (7), 3659−3853.

(19) Ross, M. O.; MacMillan, F.; Wang, J.; Nisthal, A.; Lawton, T. J.; Olafson, B. D.; Mayo, S. L.; Rosenzweig, A. C.; Hoffman, B. M. Particulate methane monooxygenase contains only mononuclear copper centers. *Science* **2019**, *364* (6440), 566.

(20) Elwell, C. E.; Gagnon, N. L.; Neisen, B. D.; Dhar, D.; Spaeth, A. D.; Yee, G. M.; Tolman, W. B. Copper−Oxygen Complexes Revisited: Structures, Spectroscopy, and Reactivity. *Chem. Rev.* **2017**, *117* (3), 2059−2107.

(21) Lewis, E. A.; Tolman, W. B. Reactivity of Dioxygen−Copper Systems. *Chem. Rev.* **2004**, *104* (2), 1047−1076.

(22) Mirica, L. M.; Ottenwaelder, X.; Stack, T. D. P. Structure and Spectroscopy of Copper−Dioxygen Complexes. *Chem. Rev.* **2004**, *104* (2), 1013−1046.

(23) Wiese, S.; Kapoor, P.; Williams, K. D.; Warren, T. H. Nitric Oxide Oxidatively Nitrosylates Ni(I) and Cu(I) C-Organonitroso Adducts. *J. Am. Chem. Soc.* **2009**, *131* (50), 18105−18111.

(24) Williams, K. D.; Cardenas, A. J. P.; Oliva, J. D.; Warren, T. H. Copper C-Nitroso Compounds: Activation of Hydroxylamines and NO Reactivity. *Eur. J. Inorg. Chem.* **2013**, *2013* (22−23), 3812−3816.

(25) Askari, M. S.; Orio, M.; Ottenwaelder, X. Controlled nitrene transfer from a tyrosinase-like arylnitroso-copper complex. *Chem. Commun.* **2015**, *51* (56), 11206−11209.

(26) Tomson, N. C.; Williams, K. D.; Dai, X.; Sproules, S.; DeBeer, S.; Warren, T. H.; Wieghardt, K. Re-evaluating the Cu K pre-edge XAS transition in complexes with covalent metal-ligand interactions. *Chem. Sci.* **2015**, *6* (4), 2474−2487.

(27) Mansuy, D.; Battioni, P.; Chottard, J. C.; Riche, C.; Chiaroni, A. Nitrosoalkane complexes of iron-porphyrins: analogy between the bonding properties of nitrosoalkanes and dioxygen. *J. Am. Chem. Soc.* **1983**, *105* (3), 455−463.

(28) Stephens, J. C.; Khan, M. A.; Nicholas, K. M. Cyclopentadienyliron complexes of nitrosobenzene: Preparation, structure and reactivity with olefins. *J. Organomet. Chem.* **2005**, *690* (21), 4727−4733.

(29) Dey, S.; Panda, S.; Ghosh, P.; Lahiri, G. K. Electronically Triggered Switchable Binding Modes of the C-Organonitroso (ArNO) Moiety on the {Ru(acac)2} Platform. *Inorg. Chem.* **2019**, *58* (2), 1627−1637.

(30) Labios, L. A.; Millard, M. D.; Rheingold, A. L.; Figueroa, J. S. Bond Activation, Substrate Addition and Catalysis by an Isolable Two-Coordinate Pd(0) Bis-Isocyanide Monomer. *J. Am. Chem. Soc.* **2009**, *131* (32), 11318−11319.

(31) Barnett, B. R.; Labios, L. A.; Moore, C. E.; England, J.; Rheingold, A. L.; Wieghardt, K.; Figueroa, J. S. Solution Dynamics of Redox Noninnocent Nitrosoarene Ligands: Mapping the Electronic Criteria for the Formation of Persistent Metal-Coordinated Nitroxide Radicals. *Inorg. Chem.* **2015**, *54* (14), 7110−7121.

(32) Matsubayashi, G.-e.; Nakatsu, K. An example of nitroso oxygen-to-metal bonding: x-ray molecular structure of dichlorodimethylbis (4-nitroso-N,N-dimethylaniline)tin(IV). *Inorg. Chim. Acta* **1982**, *64*, L163−L164.

(33) Hu, S.; Thompson, D. M.; Ikekwere, P. O.; Barton, R. J.; Johnson, K. E.; Robertson, B. E. Crystal and molecular structure of dichlorobis(4-nitroso-N,N-dimethylaniline)zinc(II), an example of an oxygen-bonded arylnitroso ligand. *Inorg. Chem.* **1989**, *28* (25), 4552−4554.

(34) Bokii, N. G.; Udel'nov, A. I.; Struchkov, Y. T.; Kravtsov, D. N.; Pachevskaya, V. M. X-ray diffraction investigation of nonbonding interactions and coordination in organometallic compounds. *J. Struct. Chem.* **1978**, *18* (6), 814−819.

(35) Fox, S. J.; Chen, L.; Khan, M. A.; Richter-Addo, G. B. Nitrosoarene Complexes of Manganese Porphyrins. *Inorg. Chem.* **1997**, *36* (27), 6465−6467.

(36) Wang, L.-S.; Chen, L.; Khan, M. A.; Richter-Addo, G. B. The first structural studies of nitrosoarene binding to iron-(II) and -(III) porphyrins. *Chem. Commun.* **1996**, No. 3, 323−324.

(37) Effaty, F.; Zsombor-Pindera, J.; Kazakova, A.; Girard, B.; Askari, M. S.; Ottenwaelder, X. Ligand and electronic effects on copper−arylnitroso self-assembly. *New J. Chem.* **2018**, *42* (10), 7758−7764.

(38) Krinninger, C.; Högg, C.; Nöth, H.; Gálvez Ruiz, J. C.; Mayer, P.; Burkacky, O.; Zumbusch, A.; Lorenz, I.-P. Dichroic, Dinuclear μ2-(η2-NO)-Nitrosoaniline-Bridged Complexes of Rhenium of the Type [{(CO)3Re(μ-X)}2ONC6H4NR2] (X = Cl, Br, I; R = Me, Et). *Chem. - Eur. J.* **2005**, *11* (24), 7228−7236.

(39) Krinninger, C.; Wirth, S.; Klüfers, P.; Mayer, P.; Lorenz, I. P. Absence of Dichroism in Dinuclear Rhenium Complexes with

https://dx.doi.org/10.1021/acs.inorgchem.9b03175
Inorg. Chem. XXXX, XXX, XXX−XXX

Sterically Hindered μ2-(η2-N,O)-Nitrosobenzene Ligands. *Eur. J. Inorg. Chem.* **2006**, *2006* (5), 1060−1066.
(40) Wilberger, R.; Krinninger, C.; Piotrowski, H.; Mayer, P.; Lorenz, I.-P. A New Dichroic, Nitroso-Bridged Complex of Rhenium: Di-μ2-chloro[μ2-(η2-N,O)-N,N-dimethyl-4-nitrosoaniline]bis-[tricarbonylrhenium(I)]. *Eur. J. Inorg. Chem.* **2004**, *2004* (12), 2488−2492.
(41) Lee, K. K. H.; Wong, W. T. Synthesis, characterization and molecular structure of a triruthenium carbonyl cluster containing both phenylimido and nitrosobenzene ligands. *J. Chem. Soc., Dalton Trans.* **1996**, No. 20, 3911−3912.
(42) Iwasa, T.; Shimada, H.; Takami, A.; Matsuzaka, H.; Ishii, Y.; Hidai, M. Preparation of Cationic Dinuclear Hydrido Complexes of Ruthenium, Rhodium, and Iridium with Bridging Thiolato Ligands and Their Reactions with Nitrosobenzene. *Inorg. Chem.* **1999**, *38* (12), 2851−2859.
(43) Packett, D. L.; Trogler, W. C.; Rheingold, A. L. Molecular structure of (.mu.-.eta.1-nitrosobenzene-N)(.mu.-.eta.2-nitrosobenzene-N,O)(.eta.1-nitrosobenzene-N)tris(trimethylphosphine)-diplatinum(II), a complex containing three linkage isomers of nitrosobenzene. *Inorg. Chem.* **1987**, *26* (26), 4308−4309.
(44) Ferretti, E.; Dechert, S.; Meyer, F. Reductive Binding and Ligand-Based Redox Transformations of Nitrosobenzene at a Dinickel(II) Core. *Inorg. Chem.* **2019**, *58* (8), 5154−5162.
(45) Liebeskind, L. S.; Sharpless, K. B.; Wilson, R. D.; Ibers, J. A. The first d0 metallooxaziridines. Amination of olefins. *J. Am. Chem. Soc.* **1978**, *100* (22), 7061−7063.
(46) Ridouane, F.; Sanchez, J.; Arzoumanian, H.; Pierrot, M. Structure of tetraphenylphosphonium tetracyanooxo[N-o-tolylhydroxylaminato(2-)-O,N]molybdate(VI). *Acta Crystallogr., Sect. C: Cryst. Struct. Commun.* **1990**, *46*, 1407−1410.
(47) Dutta, S. K.; McConville, D. B.; Youngs, W. J.; Chaudhury, M. Reactivity of Mo−Ot Terminal Bonds toward Substrates Having Simultaneous Proton- and Electron-Donor Properties: A Rudimentary Functional Model for Oxotransferase Molybdenum Enzymes. *Inorg. Chem.* **1997**, *36* (12), 2517−2522.
(48) Brouwer, E. B.; Legzdins, P.; Rettig, S. J.; Ross, K. J. Facile Nitrosyl N-O Bond Cleavage upon Thermolysis of Cp*W(NO)Ph2. *Organometallics* **1994**, *13* (5), 2088−2091.
(49) Skoog, S. J.; Campbell, J. P.; Gladfelter, W. L. Homogeneous Catalytic Carbonylation of Nitroaromatics. 9. Kinetics and Mechanism of the First N-O Bond Cleavage and Structure of the.eta.2-ArNO Intermediate. *Organometallics* **1994**, *13* (11), 4137−4139.
(50) Skoog, S. J.; Gladfelter, W. L. Activation of Nitroarenes in the Homogenous Catalytic Carbonylation of Nitroaromatics via an Oxygen-Atom-Transfer Mechanism Induced by Inner-Sphere Electron Transfer. *J. Am. Chem. Soc.* **1997**, *119* (45), 11049−11060.
(51) Pizzotti, M.; Porta, F.; Cenini, S.; Demartin, F.; Masciocchi, N. Further investigations of the reactivity of η2-bonded nitroso complexes of platinum. The crystal structure of Pt(PPh3)2(PhNO). *J. Organomet. Chem.* **1987**, *330* (1), 265−278.
(52) Kundu, S.; Stieber, S. C. E.; Ferrier, M. G.; Kozimor, S. A.; Bertke, J. A.; Warren, T. H. Redox Non-Innocence of Nitrosobenzene at Nickel. *Angew. Chem., Int. Ed.* **2016**, *55* (35), 10321−10325.
(53) Barrow, M. J.; Mills, O. S. Carbon compounds of the transition metals. Part XXI. The crystal and molecular structure of bis-[tricarbonyl-(3-chloro-2-methylnitrosobenzene)iron]. *J. Chem. Soc. A* **1971**, No. 0, 864−868.
(54) Calligaris, M.; Yoshida, T.; Otsuka, S. Preparation and structure of tris- [(tri-t-butylphosphine)(nitrosobenzene)palladium]. *Inorg. Chim. Acta* **1974**, *11*, L15−L16.
(55) Stella, S.; Floriani, C.; Chiesi-Villa, A.; Guastini, C. Side-on bonded nitrosobenzene bridging two metal atoms, in a binuclear cyclopentadienyl cobalt complex: crystal structure of [{Co(cp)}2(μ-PhNO)2]. *J. Chem. Soc., Dalton Trans.* **1988**, No. 2, 545−547.
(56) Ang, H. G.; Kwik, W. L.; Ong, K. K. Reaction of pentafluoronitrosobenzene with [Os3(CO)11(CH3CN)] and high-performance liquid chromatographic separation of [Os3(CO)11(μ-ONC6F5)], [Os3(CO)9(μ3-NC6F5)2], [Os3(CO)11(CH3CN)] and Os3(CO)12. *J. Fluorine Chem.* **1993**, *60* (1), 43−48.
(57) Hoard, D. W.; Sharp, P. R. Chemistry of [Cp*Rh(.mu.-Cl)]2 and its dioxygen and nitrosobenzene insertion products. *Inorg. Chem.* **1993**, *32* (5), 612−620.
(58) Sharp, P. R.; Hoard, D. W.; Barnes, C. L. Rhodium(II) complex with a highly reactive rhodium-rhodium bond: insertion of dioxygen and nitrosobenzene. *J. Am. Chem. Soc.* **1990**, *112* (5), 2024−2026.
(59) Scott, M. J.; Lippard, S. J. Reactivity of the Coordinated η2-Ketone in the Tropocoronand Complex [Hf(TC-3,5)(η2-OC-(CH2Ph)2)]: N−C Coupling, C−C Coupling, and Insertion into the C−O Bond. *Organometallics* **1998**, *17* (3), 466−474.
(60) Dai, X.; Kapoor, P.; Warren, T. H. [Me2NN]Co(η6-toluene): OO, NN, and ON Bond Cleavage Provides β-Diketiminato Cobalt μ-Oxo and Imido Complexes. *J. Am. Chem. Soc.* **2004**, *126* (15), 4798−4799.
(61) Mahadevan, V.; DuBois, J. L.; Hedman, B.; Hodgson, K. O.; Stack, T. D. P. Exogenous Substrate Reactivity with a [Cu(III)2O2]-2+ Core: Structural Implications. *J. Am. Chem. Soc.* **1999**, *121* (23), 5583−5584.
(62) Herres-Pawlis, S.; Verma, P.; Haase, R.; Kang, P.; Lyons, C. T.; Wasinger, E. C.; Flörke, U.; Henkel, G.; Stack, T. D. P. Phenolate Hydroxylation in a Bis(μ-oxo)dicopper(III) Complex: Lessons from the Guanidine/Amine Series. *J. Am. Chem. Soc.* **2009**, *131* (3), 1154−1169.
(63) Large, T. A. G.; Mahadevan, V.; Keown, W.; Stack, T. D. P. Selective oxidation of exogenous substrates by a bis-Cu(III) bis-oxide complex: Mechanism and scope. *Inorg. Chim. Acta* **2019**, *486*, 782−792.
(64) Chen, P.; Root, D. E.; Campochiaro, C.; Fujisawa, K.; Solomon, E. I. Spectroscopic and Electronic Structure Studies of the Diamagnetic Side-On CuII-Superoxo Complex Cu(O2)[HB(3-R-5-iPrpz)3]: Antiferromagnetic Coupling versus Covalent Delocalization. *J. Am. Chem. Soc.* **2003**, *125* (2), 466−474.
(65) Ginsbach, J. W.; Peterson, R. L.; Cowley, R. E.; Karlin, K. D.; Solomon, E. I. Correlation of the Electronic and Geometric Structures in Mononuclear Copper(II) Superoxide Complexes. *Inorg. Chem.* **2013**, *52* (22), 12872−12874.
(66) Woertink, J. S.; Tian, L.; Maiti, D.; Lucas, H. R.; Himes, R. A.; Karlin, K. D.; Neese, F.; Würtele, C.; Holthausen, M. C.; Bill, E.; Sundermeyer, J. r.; Schindler, S.; Solomon, E. I. Spectroscopic and Computational Studies of an End-on Bound Superoxo-Cu(II) Complex: Geometric and Electronic Factors That Determine the Ground State. *Inorg. Chem.* **2010**, *49* (20), 9450−9459.
(67) Noh, H.; Cho, J. Synthesis, characterization and reactivity of non-heme 1st row transition metal-superoxo intermediates. *Coord. Chem. Rev.* **2019**, *382*, 126−144.
(68) Solomon, E. I. Dioxygen Binding, Activation, and Reduction to H2O by Cu Enzymes. *Inorg. Chem.* **2016**, *55* (13), 6364−6375.
(69) Mason, J.; Larkworthy, L. F.; Moore, E. A. Nitrogen NMR Spectroscopy of Metal Nitrosyls and Related Compounds. *Chem. Rev.* **2002**, *102* (4), 913−934.
(70) Mugnier, Y.; Gard, J. C.; Huang, Y.; Couture, Y.; Lasia, A.; Lessard, J. Electrochemically induced chain reactions: the electrochemical behavior of nitrosobenzene in the presence of proton donors in tetrahydrofuran. *J. Org. Chem.* **1993**, *58* (20), 5329−5334.
(71) Asirvatham, M. R.; Hawley, M. D. Electron-transfer processes: The electrochemical and chemical behavior of nitrosobenzene. *J. Electroanal. Chem. Interfacial Electrochem.* **1974**, *57* (2), 179−190.
(72) Núñez-Vergara, L. J.; Squella, J. A.; Olea-Azar, C.; Bollo, S.; Navarrete-Encina, P. A.; Sturm, J. C. Nitrosobenzene: electrochemical, UV-visible and EPR spectroscopic studies on the nitrosobenzene free radical generation and its interaction with glutathione. *Electrochim. Acta* **2000**, *45* (21), 3555−3561.
(73) De Leener, G.; Over, D.; Smet, C.; Cornut, D.; Porras-Gutierrez, A. G.; López, I.; Douziech, B.; Le Poul, N.; Topić, F.; Rissanen, K.; Le Mest, Y.; Jabin, I.; Reinaud, O. Two-Story" Calix[6]arene-Based Zinc and Copper Complexes: Structure, Properties, and O2 Binding. *Inorg. Chem.* **2017**, *56* (18), 10971−10983.

https://dx.doi.org/10.1021/acs.inorgchem.9b03175
Inorg. Chem. XXXX, XXX, XXX−XXX

(74) Kindermann, N.; Günes, C.-J.; Dechert, S.; Meyer, F. Hydrogen Atom Abstraction Thermodynamics of a μ-1,2-Superoxo Dicopper-(II) Complex. *J. Am. Chem. Soc.* **2017**, *139* (29), 9831−9834.
(75) López, I.; Cao, R.; Quist, D. A.; Karlin, K. D.; Le Poul, N. Direct Determination of Electron-Transfer Properties of Dicopper-Bound Reduced Dioxygen Species by a Cryo-Spectroelectrochemical Approach. *Chem. - Eur. J.* **2017**, *23* (72), 18314−18319.
(76) López, I.; Porras-Gutiérrez, A. G.; Douziech, B.; Wojcik, L.; Le Mest, Y.; Kodera, M.; Le Poul, N. O−O bond cleavage via electrochemical reduction of a side-on peroxo dicopper model of hemocyanin. *Chem. Commun.* **2018**, *54* (39), 4931−4934.
(77) Halvagar, M. R.; Solntsev, P. V.; Lim, H.; Hedman, B.; Hodgson, K. O.; Solomon, E. I.; Cramer, C. J.; Tolman, W. B. Hydroxo-Bridged Dicopper(II,III) and -(III,III) Complexes: Models for Putative Intermediates in Oxidation Catalysis. *J. Am. Chem. Soc.* **2014**, *136* (20), 7269−7272.
(78) Ali, G.; VanNatta, P. E.; Ramirez, D. A.; Light, K. M.; Kieber-Emmons, M. T. Thermodynamics of a μ-oxo Dicopper(II) Complex for Hydrogen Atom Abstraction. *J. Am. Chem. Soc.* **2017**, *139* (51), 18448−18451.
(79) Isaac, J. A.; Gennarini, F.; López, I.; Thibon-Pourret, A.; David, R.; Gellon, G.; Gennaro, B.; Philouze, C.; Meyer, F.; Demeshko, S.; Le Mest, Y.; Réglier, M.; Jamet, H.; Le Poul, N.; Belle, C. Room-Temperature Characterization of a Mixed-Valent μ-Hydroxodicopper-(II,III) Complex. *Inorg. Chem.* **2016**, *55* (17), 8263−8266.
(80) Thibon-Pourret, A.; Gennarini, F.; David, R.; Isaac, J. A.; Lopez, I.; Gellon, G.; Molton, F.; Wojcik, L.; Philouze, C.; Flot, D.; Le Mest, Y.; Réglier, M.; Le Poul, N.; Jamet, H.; Belle, C. Effect of Monoelectronic Oxidation of an Unsymmetrical Phenoxido-Hydroxido Bridged Dicopper(II) Complex. *Inorg. Chem.* **2018**, *57* (19), 12364−12375.
(81) Gennarini, F.; David, R.; López, I.; Le Mest, Y.; Réglier, M.; Belle, C.; Thibon-Pourret, A.; Jamet, H.; Le Poul, N. Influence of Asymmetry on the Redox Properties of Phenoxo- and Hydroxo-Bridged Dicopper Complexes: Spectroelectrochemical and Theoretical Studies. *Inorg. Chem.* **2017**, *56* (14), 7707−7719.
(82) Shearer, J.; Zhang, C. X.; Zakharov, L. N.; Rheingold, A. L.; Karlin, K. D. Substrate Oxidation by Copper−Dioxygen Adducts: Mechanistic Considerations. *J. Am. Chem. Soc.* **2005**, *127* (15), 5469−5483.
(83) Warren, J. J.; Tronic, T. A.; Mayer, J. M. Thermochemistry of Proton-Coupled Electron Transfer Reagents and its Implications. *Chem. Rev.* **2010**, *110* (12), 6961−7001.
(84) Cappellani, E. P.; Drouin, S. D.; Jia, G.; Maltby, P. A.; Morris, R. H.; Schweitzer, C. T. Effect of the Ligand and Metal on the pKa Values of the Dihydrogen Ligand in the Series of Complexes [M(H2)H(L)2]+, M = Fe, Ru, Os, Containing Isosteric Ditertiaryphosphine Ligands, L. *J. Am. Chem. Soc.* **1994**, *116* (8), 3375−3388.
(85) Bailey, W. D.; Dhar, D.; Cramblitt, A. C.; Tolman, W. B. Mechanistic Dichotomy in Proton-Coupled Electron-Transfer Reactions of Phenols with a Copper Superoxide Complex. *J. Am. Chem. Soc.* **2019**, *141* (13), 5470−5480.
(86) Mandal, M.; Elwell, C. E.; Bouchey, C. J.; Zerk, T. J.; Tolman, W. B.; Cramer, C. J. Mechanisms for Hydrogen-Atom Abstraction by Mononuclear Copper(III) Cores: Hydrogen-Atom Transfer or Concerted Proton-Coupled Electron Transfer? *J. Am. Chem. Soc.* **2019**, *141* (43), 17236−17244.
(87) Kubas, G. J.; Monzyk, B.; Crumblis, A. L. Tetrakis-(acetonitrile)copper(1+) hexafluorophosphate(1-). *Inorg. Synth.* **2007**, *28*, 68−70.
(88) Wu, G.; Zhu, J.; Mo, X.; Wang, R.; Terskikh, V. Solid-State 17O NMR and Computational Studies of C-Nitrosoarene Compounds. *J. Am. Chem. Soc.* **2010**, *132* (14), 5143−5155.
(89) Heying, R. S.; Nandi, L. G.; Bortoluzzi, A. J.; Machado, V. G. A novel strategy for chromogenic chemosensors highly selective toward cyanide based on its reaction with 4-(2,4-dinitrobenzylideneamino)-benzenes or 2,4-dinitrostilbenes. *Spectrochim. Acta, Part A* **2015**, *136*, 1491−1499.
(90) Priewisch, B.; Rück-Braun, K. Efficient Preparation of Nitrosoarenes for the Synthesis of Azobenzenes. *J. Org. Chem.* **2005**, *70* (6), 2350−2352.
(91) Halasz, I.; Biljan, I.; Novak, P.; Meštrović, E.; Plavec, J.; Mali, G.; Smrečki, V.; Vančik, H. Cross-dimerization of nitrosobenzenes in solution and in solid state. *J. Mol. Struct.* **2009**, *918* (1−3), 19−25.
(92) Neese, F. The ORCA program system. *Wiley Interdiscip. Rev.: Comput. Mol. Sci.* **2012**, *2* (1), 73−78.
(93) Perdew, J. P. Erratum: Density-functional approximation for the correlation energy of the inhomogeneous electron gas. *Phys. Rev. B: Condens. Matter Mater. Phys.* **1986**, *34* (10), 7406.
(94) Perdew, J. P. Density-functional approximation for the correlation energy of the inhomogeneous electron gas. *Phys. Rev. B: Condens. Matter Mater. Phys.* **1986**, *33* (12), 8822.
(95) Becke, A. D. Density-functional exchange-energy approximation with correct asymptotic behavior. *Phys. Rev. A: At., Mol., Opt. Phys.* **1988**, *38* (6), 3098−3100.
(96) Schäfer, A.; Huber, C.; Ahlrichs, R. Fully optimized contracted Gaussian basis sets of triple zeta valence quality for atoms Li to Kr. *J. Chem. Phys.* **1994**, *100* (8), 5829−5835.
(97) Neese, F. An improvement of the resolution of the identity approximation for the formation of the Coulomb matrix. *J. Comput. Chem.* **2003**, *24* (14), 1740−1747.
(98) Weigend, F. Accurate Coulomb-fitting basis sets for H to Rn. *Phys. Chem. Chem. Phys.* **2006**, *8* (9), 1057−1065.
(99) *Chemcraft*, http://chemcraftprog.com.
(100) Klamt, A.; Schüürmann, G. COSMO: a new approach to dielectric screening in solvents with explicit expressions for the screening energy and its gradient. *J. Chem. Soc., Perkin Trans. 2* **1993**, No. 5, 799−805.
(101) Casida, M. Time-Dependent Density Functional Response Theory for Molecules. *Recent Advances in Density Functional Methods*; World Scientific, 1995; Vol. *1*, pp 155−192.
(102) Stratmann, R. E.; Scuseria, G. E.; Frisch, M. J. An efficient implementation of time-dependent density-functional theory for the calculation of excitation energies of large molecules. *J. Chem. Phys.* **1998**, *109* (19), 8218−8224.
(103) Bauernschmitt, R.; Ahlrichs, R. Treatment of electronic excitations within the adiabatic approximation of time dependent density functional theory. *Chem. Phys. Lett.* **1996**, *256* (4), 454−464.
(104) Hirata, S.; Head-Gordon, M. Time-dependent density functional theory within the Tamm−Dancoff approximation. *Chem. Phys. Lett.* **1999**, *314* (3), 291−299.
(105) Hirata, S.; Head-Gordon, M. Time-dependent density functional theory for radicals: An improved description of excited states with substantial double excitation character. *Chem. Phys. Lett.* **1999**, *302* (5), 375−382.
(106) Neese, F. Prediction of electron paramagnetic resonance g values using coupled perturbed Hartree−Fock and Kohn−Sham theory. *J. Chem. Phys.* **2001**, *115* (24), 11080−11096.

https://dx.doi.org/10.1021/acs.inorgchem.9b03175
Inorg. Chem. XXXX, XXX, XXX−XXX